ISBN: 978-3-95450-202-8 doi:10.18429/JACoW-HB2018-TUP2WE02

THE BEAM CONDITIONS ON THE TARGET AND ITS OPERATIONAL IMPACTS ON BEAM INTERCEPTING DEVICES AT EUROPEAN SPALLATION SOURCE

Y. Lee*, R. Miyamoto, T. Shea, European Spallation Source ERIC, SE-225 92 Lund, Sweden
H. D. Thomsen, ISA - Centre for Storage Ring Facilities, DK-8000 Aarhus, Denmark

Abstract

A large flux of spallation neutrons will be produced at the European Spallation Source (ESS) by impinging high power proton beam on the tungsten target. Until the 5 MW proton beam is stopped by the spallation target, it travels through a number of beam intercepting devices (BIDs), which include the proton beam window, a multi-wire beam profile monitor, an aperture monitor, the beam entrance window, spallation material and the target shroud. The beam-induced thermo-mechanical loads and the damage dose rate in the BIDs are largely determined by the beam energy and the beam current density. At ESS, the proton beam energy will be commissioned step-wisely, from 571 MeV towards 2 GeV. The beam current density on the BIDs in the target station is uniformly painted by raster beam optics. The ESS Linac and its beam optics will create rectangular beam profiles on the target with varying beam intensities. In this paper, we study the impact of different plausible beam intensities and beam energies on the thermo-mechanical loads and radiation damage rates in the BIDs at the ESS target station.

INTRODUCTION

Upon full commissioning of the European Spallation Source (ESS) in the next decade, the spallation target will receive 5 MW beam from the linac [1, 2]. For a reliable operation of the facility, it is crucial to keep structural integrity of the beam intercepting devices (BIDs) under the dynamic load induced by the beam pulses with 4% duty cycle and occasional beam trips. From a maintenance viewpoint, it is important to achieve a longest possible lifetime of these devices under radiation damage. The BIDs under heavy proton beam load are the spallation target, the proton beam window (PBW), and the multi-wire profile monitor (MWPM).

The dynamic beam load on the BIDs can be reduced by creating a uniform beam spot with a reduced beam current density. This slows down the radiation damage rate and lowers the cyclic thermo-mechanical load, prolonging the lifetimes of the BIDs. In order to create a uniform beam footprint on the BIDs, the ESS applies a raster system that sweeps the beam in a transverse pattern. The dimension of the raster area and the size of the beam determine the radiation damage and beam induced thermo-mechanical loads on the BIDs. A focused raster area and beam intensity cause a higher damage and heat deposition intensity in the BIDs. On the contrary, widely spanned raster beam causes a high level of beam loss from the PBW to the target, as the PBW induces a beam divergence via multiple scattering.

Besides the beam intensity, the radiation damage rate and heat deposition also depend on the beam energy. The ESS beam energy will be ramped up step-wisely from 571 MeV towards 2 GeV upon commissioning, with installation of additional cryomodules during long shut down periods. It is important to know the correlation between the beam conditions and the material behaviour of the BIDs, in assessing the system reliability and the service lifetime.

In this paper, we study the impact of different plausible beam intensities and beam energies on the thermo-mechanical loads and radiation damage rates in the BIDs at ESS.

BEAM INTERCEPTING DEVICES AT TARGET STATION

Once the proton beam enters the target station, it passes through PBW, MWPM, and beam entrance window (BEW) in a sequence until the beam is finally stopped by the tungsten spallation volume. Each of these beam intercepting devices are introduced in the following.

Proton Beam Window

The PBW is located at 3.5 meter upstream beam direction of the target. It interfaces to accelerator vacuum and serves as the gate for the incoming proton beam to target. The PBW consists of two convex plates made of Al6061-T651, which are 1 mm (upstream window) and 1.25 mm (downstream window) thin respectively. The precipitation hardened aluminium alloy is chosen, due to its low scattering cross-sections to incoming proton beam, good radiation resistance and good mechanical strength. The deposited beam power in the PBW is removed by the water flow running between the two plates.

Multiwire Beam Profile Monitor

The Multiwire Beam Profile Monitor (MWPM) is located 1.7 meter upstream of the target. It consists of five layers of horizontal, vertical, and diagonal wires. Each wire for the beam interception is made of SiC and has a diameter of 100 μm. It measures the position, profile, and peak density of the high intensity proton beam traveling to the spallation target.

Beam Entrance Window

The tungsten spallation volume is contained in the gas-tight target vessel. The BEW is a part of the target vessel

* yongjoong.lee@esss.se

ISBN: 978-3-95450-202-8 doi:10.18429/JACoW-HB2018-TUP2WE02

which faces the impinging proton beam. It is made of solution annealed 316L type stainless steel material, due to its proven lifetime under high power proton irradiation environments. The BEW is cooled by gaseous helium jet flow.

Tungsten Bricks

The spallation volume of the target consists of 6696 tungsten bricks. Each brick is 10 mm in width, 30 mm in depth and 80 mm in height. The spacing between two adjacent bricks is 2 mm. Figure 1 shows the layout of tungsten bricks placed on the cassette. Maximum 16 tungsten bricks span

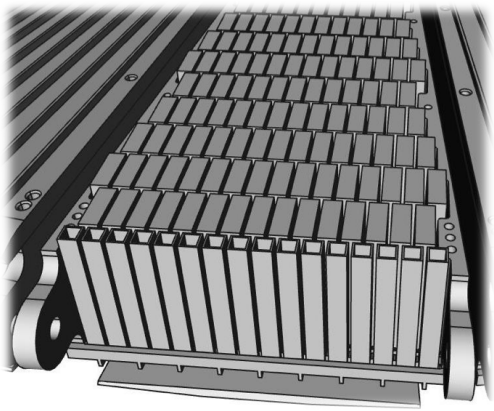

Figure 1: Layout of tungsten bricks in the cassette.

190 mm horizontally in each target segment. Each brick is held by top and bottom cassette plates, which shadow 10 mm of 80 mm height of the tungsten bricks. Therefore, the view area of the tungsten spallation volume seen by the proton beam is defined by -95 mm $\leq x \leq +95$ mm and -35 mm $\leq y \leq +35$ mm.

BEAM RASTER PARAMETER

Target Area Definition

Ideally, should all the incoming protons land on the tungsten spallation volume, while not hitting the structural parts made of stainless steel. The beam footprint on the target may deviate from the centre point of the segment by maximum ±14.7 mm horizontally and by maximum ±3.0 mm vertically [3]. The front face of the tungsten is 1250 mm in distance from the rotation axis of the target wheel. The target wheel rotates with a frequency of 14/36 Hz, and the front face of the tungsten drifts by 9 mm during the pulse length of 2.86 ms. The requirement on the positioning accuracy of beam footprint on target is set to be less than ±5 mm. The horizontal runout of the target wheel is maximum ±2.4 mm. The tolerance on the horizontal displacement of the wheel position is limited by ±2.0 mm. The phase error from the target rotation speed contributes to maximum ±2.0 mm horizontal deviation of the beam footprint from its centre position. The vertical deviation is mainly contributed by the positioning accuracy of beam footprint on target, which is set to be less than ±3 mm.

Taking the maximum beam deviations from the centre point of each segment into account, the effective view area of tungsten by the proton beam is reduced from the ideal view area of 190×70 mm^2 to 160×64 mm^2.

Nominal Raster Parameter

The raster magnet system generates a Lissajous-like pattern using triangular wave forms to create a two dimensional mesh of interweaved sweep trajectories. During the beam pulse starting at the time $t = t_0$, the trajectory of the beam centroid in the plane perpendicular to the beam direction at the BEW is described by

$$x_i(\tilde{t}) = \Delta_i \left[4 \left| \mod \left(\frac{n_i \tilde{t}}{\tau} - \phi_i,\ 1 \right) - \frac{1}{2} \right| - 1 \right], \quad (1)$$

for $i = x,\ y$ and $\tilde{t} \equiv t - t_0$. Here, τ represents the beam pulse length, and Δ_x and Δ_y respectively represent the raster amplitudes in the horizontal and vertical directions. The parameters n_x and n_y represent the number of sweeps during the beam pulse respectively in the horizontal and vertical directions. These are correlated to the raster frequency f_x and f_y via $n_i = f_i \cdot \tau$. The ϕ_is are free parameters representing phase shifts. Table 1 summarises the nominal beam raster parameters at the BEW.

Table 1: Nominal Beam Raster Parameters on the BEW

Parameter	Symbol	Value	Unit
Pulse length	τ	2.86	[ms]
Maximum displacements	Δ_x	60.0	[mm]
	Δ_y	20.0	[mm]
Sweep frequency	f_x	39.55	[kHz]
	f_y	29.05	[kHz]

BEAM FRACTION ON TARGET FOR DIFFERENT BEAM ENERGIES

Proton Scattering at PBW

The protons are lost on its way to the target. The main cause of loss is the multiple scattering at the PBW. The extent of proton scattering depends on the beam energy. Three beam energies are considered, the 571 MeV, 1300 MeV and 2 GeV. When the linac unit up to the medium beta cryomodules is fully functional, a 571 MeV beam will be delivered to the target. The 1.3 GeV beam will be delivered when about a half of the high beta cryomodules are commissioned. With a full commissioning of the linac, a 2 GeV beam will be delivered to the target.

In order to calculate the additional beam divergence due to the presence of the PBW, Monte-Carlo simulations are made using FLUKA [4, 5]. The beam source distribution at 6 meters upstream of the target is calculated by TraceWin [6], which is then read by FLUKA for particle transport simulations. Figure 2 shows the angular distribution of the proton

ISBN: 978-3-95450-202-8 doi:10.18429/JACoW-HB2018-TUP2WE02

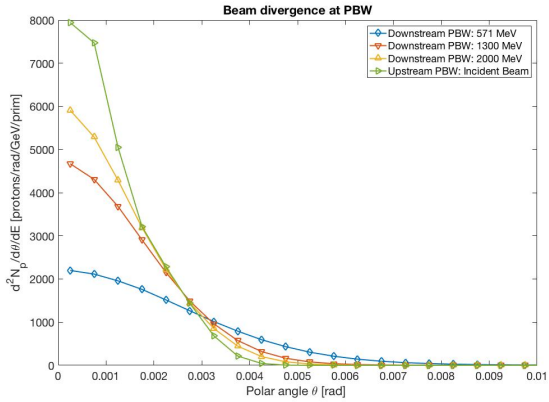

Figure 2: The polar angle distribution of proton momentum upstream and downstream of the PBW.

momentum upstream and downstream of the PBW. For reference, a polar angle divergence of 1.0 mrad implies a 3.5 mm transverse offset on the target. The simulation shows that about 1 % of the protons are lost at the PBW, depositing about 2 MeV per proton in there.

By tracing the free particle trajectories which are scattered by the PBW, the fraction of beam that land on the target area 160×64 mm^2 on the tungsten bricks are calculated, for different beam energies. The energy dependence of beam loss on the target is summarised in Table 2. In order to show the beam loss due to scattering at the PBW, MWPM and BEW, a reference case is also shown, which assumes no beam interception in the upstream beamline of the target.

Table 2: The Fraction of Beam that Land on the Target Area

Beam energy	Fraction on target	Reference fraction	Statistical Error
0.571 GeV	0.885	0.961	±0.01%
1.300 GeV	0.928	0.961	±0.01%
2.000 GeV	0.965	0.988	±0.01%

Compared to the reference fraction, which is determined by linac optics and raster parameters, the presence of BIDs causes additional beam losses of 2% for a 2 GeV beam, 3% for a 1.3 GeV beam and 7% for a 571 MeV beam. The deviations from the reference beam loss could be reduced if the collimation effect of the proton channel surrounded by the monolith shielding structure is taken into account. Further analysis will be made to fine-tune the raster parameters further, for different proton beam energies.

Beam Loss and Thermal Stress in Target Vessel

If the beam on target suffers from maximum allowed offset, the maximum heat deposition at the target boundary per pulse is calculated to be less than 10 MJ·m^{-3} in stainless steel. If the edge of the raster boundary misses tungsten bricks and hits the target vessel structure instead, the maximum temperature increase in the steel structure is calculated to be less than 3 °C per pulse. This temperature increase per pulse makes the 316L stainless steel to expand by 4.8 μm·m^{-1}, resulting in less than 10 MPa additional thermal stress, which is about 5% of the yield stress. From this, we conclude that protons landing off the target area do not risk the structural integrity of the target wheel.

EFFECTS OF BEAM SIZE

Raster Failure and Heat in PBW and BEW

In case beam raster fails completely, a single beam deposits a concentrated heat load in the PBW and BEW. During a single full power pulse, the maximum temperature increases by $\Delta T_{\max}$ in the PBW and BEW are expressed by

$$\Delta T_{\max} = \frac{\tau}{\rho C_{\mathrm{p}}} \frac{i_{\mathrm{total}}}{2\pi\sigma_x\sigma_y} \left.\frac{dE}{dz}\right|_{\max} . \qquad (2)$$

Here, τ is the pulse length, ρ is the mass density, C_{p} is the specific heat, i_{total} is the beam current, the $dE/dz|_{\max}$ is the maximum energy deposition per single incident proton per unit length, and σ_x and σ_y are the beam RMS sizes.

A requirement on the beam size is that the structural functionality of the PBW and BEW shall not change with a failure of beam raster for single pulse. The aluminium alloy Al6061-T651 of which the PBW is made overages if the temperature on it temporarily reaches above 250 °C [7]. Therefore, the temperature in the PBW shall not increase above $T_{\mathrm{max:PBW}}$ =250 °C during single pulse. On the other hand, a prolonged exposure to temperatures in the range of 550 °C to °850 C in austenitic steel may cause chromium-rich carbides to precipitate at the grain boundaries. This limits the maximum temperature in the BEW to be below $T_{\mathrm{max:BEW}}$ =550 °C.

The maximum operational temperatures in the PBW and BEW are 60 °C and 160 °C respectively. The threshold beam sizes to raise the maximum temperatures above $T_{\mathrm{max:PBW}}$ and $T_{\mathrm{max:BEW}}$ are calculated to be $\sigma_x \cdot \sigma_y = 33.5$ mm^2 on BEW and $\sigma_x \cdot \sigma_y = 32.6$ mm^2 on PBW. The nominal beam cross sections are $\sigma_x \cdot \sigma_y = 68.2$ mm^2 on BEW and $\sigma_x \cdot \sigma_y = 42.5$ mm^2 on PBW, satisfying the requirements with a safety margin of 30%.

Dynamic Stress Wave in Tungsten Bricks

The raster sweep during beam pulse induces dynamic stress wave in the tungsten bricks inside the target. For the nominal beam size and raster parameters, each sweep of beam raster on a tungsten brick induces an effective pulsed beam load with a few microseconds' pulse length.

Coupled thermal and transient structural simulations are made for a tungsten brick for 30 beam raster sweeps, using ANSYS Workbench [8]. Two different beam sizes are considered, the nominal one with $\sigma_x \times \sigma_y = 13.5 \times 5.05$ mm^2, and the one with $\sigma_x \times \sigma_y = 10.8 \times 4.04$ mm^2 having 40% higher beam intensity. Figure 3 shows the dynamic transient and quasi-static von Mises stress responses of a tungsten brick located at the centre of a target wheel segment.

ISBN: 978-3-95450-202-8 doi:10.18429/JACoW-HB2018-TUP2WE02

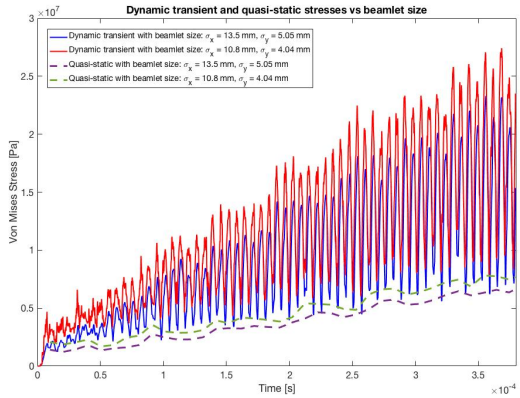

Figure 3: The dynamic transient and quasi-static von Mises stress responses of a tungsten brick located at the centre of a target wheel segment.

With a smaller beam size, the stress amplitude gets higher. This should be due to higher beam intensity combined with shorter beam exposure time per raster sweep. The amplitudes of dynamic transient stresses amplify with time, without showing a sign of saturation. The peak transient stress during the simulated time interval is almost 4 times higher than that of quasi-static stress. The reason for this could be attributed to proximity of the multiples of horizontal raster frequency f_{raster} =39.55 kHz to the resonance frequency of the tungsten brick. The calculated resonance modes are at the frequencies of 41.2 kHz (1.04 f_{raster}) and 78.4 kHz (1.98 f_{raster}). The coherence between the resonance frequency and the beam raster sweep rate will be further analysed. The raster parameters will be fine tuned to avoid the raster sweep rate lies within a band-width of a resonance mode of tungsten bricks.

HEAT LOADS AND BEAM ENERGIES

The heat deposition in the BIDs differ for different beam energies. Table 3 summarises the calculated maximum beam energy per single proton deposited in the beam intercepting materials. For the same beam current, the beam energy deposited in the BEW and tungsten bricks increase with beam energy. This is due to larger contribution of back scattered neutrons from the dense spallation volume at higher beam energies. However, the heat deposited in the PBW is the highest at 571 MeV, which is about 16% higher than that of the 2 GeV beam. At the early stage of the linac commissioning with a lower energy beam, an attention should be paid to this higher heat load and associated higher thermal stress in the PBW.

Table 3: Calculated Beam Stopping Power per Single Proton in the Beam Intercepting Materials

Beam Energy [GeV]	PBW	BEW	Tungsten (Max.)
	[MeV·proton^{-1}]		
0.571	1.41	3.98	8.12
1.300	1.24	4.38	10.8
2.000	1.22	5.01	14.5

RADIATION DAMAGE

Proton Beam Window

The proton dose limited lifetime of the PBW is determined by the helium production in the aluminium alloy [9]. The helium production rate depends on proton energy and beam current density. At ESS, the total helium production in the aluminium alloy is limited by 2400 He-appm. FLUKA simulations are performed to calculate the helium production rate in the PBW. In steady operation, full current beam will be delivered to the target for 5400 hours per year. With the maximum time averaged beam current of 2.5 mA, the calculated accumulated helium production in the PBW per year are respectively 2240 appm at 571 MeV, 3160 appm at 1.3 GeV and 3620 appm at 2.0 GeV. Applying the maximum 2400 He-appm criterion in the PBW, the lifetimes of the PBW are respectively 5780 hours (8.25 GWh of accumulated beam energy) at 571 MeV, 4110 hours (13.3 GWh of accumulated beam energy) at 1.3 GeV, and 3580 hours (17.9 GWh of accumulated beam energy) at 2.0 GeV.

Beam Entrance Window

The maximum displacement damage on the BEW made of stainless steel 316L is 0.4 dpa at 2 GeV, 0.35 dpa at 1.3 GeV and 0.25 dpa at 571 MeV for the 5400 hours of annual operation at full current. During the 5 year lifetime of the target wheel, the BEW will receive less than 2.5 dpa of the damage dose, which is more than three times less than the maximum displacement damage dose recorded in the SNS target window [10]. Indeed, the maximum displacement dose in the ESS target wheel is located at the horizontal vessel plates mainly due to a high intensity fast neutron flux [11]. The lifetime of the target wheel is limited by the maximum displacement dose of 7.5 dpa in the target wheel during 5 years of full power operation. With a lower beam energy than 2.0 GeV, the target lifetimes are extrapolated to be 6 years at 1.3 GeV and 8 years at 571 MeV.

Spallation Material

As the spallation material does not carry any structural function, there is no dose limited lifetime defined for the tungsten. The calculated maximum displacement damage in the tungsten bricks are 1.0 dpa/year at 571 MeV, 3.0 dpa/year at 1.3 GeV and 2.6 dpa/year at 2.0 GeV. Tungsten is known to show completely brittle behaviour at the operational temperature of 500 °C already at above 0.1 dpa [12]. With the proton and neutron induced radiation damage, the thermal conductivity will also degrade with time [13]. The radiation damage in tungsten also makes the material stiffer. Pure tungsten irradiated by heavy ion up to the maximum damage level of 0.05 dpa showed an increased material stiffness by 12% [14].

ISBN: 978-3-95450-202-8 doi:10.18429/JACoW-HB2018-TUP2WE02

The effect of radiation induced changes of thermal conductivity and stiffness on the operational temperature and related static stress level in the tungsten brick has been studied with FLUKA and ANSYS simulations. The temperature dependent thermal conductivity of irradiated tungsten is taken from Ref. [13] for 3.8 dpa, and 20% higher Young's modulus has been assumed for the irradiated tungsten based on Ref. [14]. The results of analyses, based on a quarter of single wheel segment model shown in Fig. 4, are summarised in Table 4. Specifically, a transient simulation for 10 beam pulses are made, where the initial condition is provided by a calculated steady state configuration.

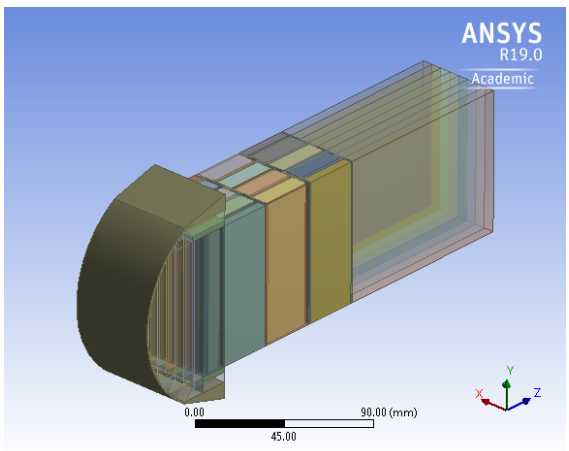

Figure 4: The geometry model used for the flow simulations, which represent a quarter of single target wheel segment.

Table 4: Radiation Damage Effect on Operation Temperature and Maximum von Mises Stress in a Tungsten Brick

Parameter	Time	Unirr.	Irrad.
maximum temperature	Pre-pulse	321 °C	337 °C
	Post-pulse	395 °C	411 °C
maximum stress	Pre-pulse	27 MPa	50 MPa
	Post-pulse	83 MPa	117 MPa

Also the effect of different raster sweep areas is analysed. For an un-irradiated tungsten brick, the reduced maximum raster amplitudes Δ_x =54.3 mm and Δ_y =18.7 mm result in higher temperatures and thermal stresses. The calculated pre and post-pulse temperatures are 341 °C and 427 °C respectively, showing a marginal increase of temperature compared to the nominal beam case. The corresponding von Mises stresses are 31 MPa and 117 MPa respectively, which are considerably larger than the nominal beam case. This shows that the beam raster area need to be monitored with an order of milli-meter scale precision to avoid a higher than design stress in tungsten bricks.

Multiwire Beam Profile Monitor

At 5 MW proton beam power with nominal raster parameters, the displacement damage in the MWPM made of SiC is 5 dpa per year. A highest damage level in SiC wires for beam profile monitoring is known to be deposited at Target Station 2 of ISIS, which is estimated to be 3 dpa and it continues operating without failure. Based on this, the proton damage lifetime of the MWPM is estimated to be 1 year at 5 MW operation of proton beam at ESS.

NEUTRON YIELDS FOR DIFFERENT BEAM ENERGIES

In order to assess the neutron yield from the target, a toy FLUKA model consisting of a tungsten slab with dimension 180×80×400 mm^3 subject to a pencil beam is studied. Figure 5 shows the energy dependent spallation neutron flux from the top and bottom surfaces of the tungsten slab per MW beam power.

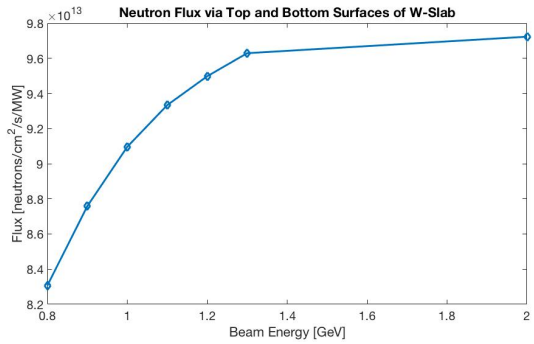

Figure 5: The energy dependent spallation neutron flux from the top and bottom surfaces of the tungsten slab per MW beam power.

The flux of spallation neutron per unit power increases with the beam energy, until it saturates at above 1.3 GeV. This loss of spallation neutron flux at lower beam energies can be compensated to a certain extent by optimising moderators and reflectors [15].

CONCLUSIONS

The correlation between the beam parameters on the target and its implications on the operational conditions of the beam intercepting devices are studied. The thermo-mechanical loads on the BIDs could differ considerably with a minor change of beam parameters, which shows the importance of beam diagnostics with precision. The beam parameters will be further fine-tuned from its baseline values, to gain higher reliability of the BIDs than is predicted under nominal beam parameters.

REFERENCES

[1] S. Peggs *et al.*, "ESS Technical Design Report", ISBN 978-91-980173-2-8 in ESS-doc-274, April 2013.

[2] R. Garoby *et al.*, "The European Spallation Source design", *Phys. Scr.* vol. 93, pp. 014001, 2018, doi:10.1088/1402-4896/aa9bff

ISBN: 978-3-95450-202-8 doi:10.18429/JACoW-HB2018-TUP2WE02

[3] K. Sjögreen, "WP2 Target wheel, drive and shaft description of operational limits", Technical Report ESS-0084036, European Spallation Source ERIC, 2018.

[4] A. Ferrari, P. R. Sala, A. Fassò, and J. Ranft, "FLUKA: a multi-particle transport code", CERN-2005-10, INFN/TC_05/11, SLAC-R-773, 2005.

[5] T. T. Böhlen, F. Cerutti, M. P. W. Chin, A. Fassò, A. Ferrari, P. G. Ortega, A. Mairani, P. R. Sala, G. Smirnov, and V. Vlachoudis, "The FLUKA Code: Developments and Challenges for High Energy and Medical Applications", *Nuclear Data Sheets*, vol. 120, pp. 211–214, 2014, doi:10.1016/j.nds.2014.07.049

[6] R. Duperrier, N. Pichoff, and D. Uriot, "Saclay Codes Review for High Intensities Linacs Computations", in *Proc. ICCS'02*, pp. 411-418, 2002.

[7] "RCC-MRx: Design and Construction Rules for Mechanical Components of Nuclear Installations", ISBN 2-913638-40-6, AFCEN, 2012 Edition, 2012.

[8] ANSYS® Academic Research Workbench, Release 19.0, ANSYS, Inc.

[9] Y. Dai and D. Hamaguchi, "Mechanical Properties and Microstructure of $AlMg_3$ Irradiated in SINQ Target-3", *Journal of Nuclear Materials*, vol. 343, pp. 184–190, 2005, doi:10.1016/j.jnucmat.2004.11.021

[10] B. J. Vevera, D. A. McClintock, J. W. Hyres, and B. W. Riemer, "Characterization of Irradiated AISI 316L Stainless Steel Disks Removed from the Spallation Neutron Source", *Journal of Nuclear Materials*, vol. 450, pp. 147–162, 2014, doi:10.1016/j.jnucmat.2014.02.035

[11] F. Sordo *et al.*, "Radiation Damage Analysis for the ESS Target", Technical Report ESS-0037287, ESS-Bilbao, 2017.

[12] H. Ullmaier and F. Carsughi, "Radiation Damage Problems in High Power Spallation Neutron Sources", *Nuclear Instruments and Methods in Physics Research* B, vol. 101, pp. 406–421, 1995, doi:10.1016/0168-583X(95)00590-0

[13] J. Habainy, Y. Dai, Y. Lee, and S. Iyengar, "Thermal Diffusivity of Tungsten Irradiated with Protons up to 5.8 dpa", *Journal of Nuclear Materials*, submitted.

[14] J. Habainy, Y. Lee1, K. B. Surreddi, A. Prosvetov, P. Simon, S. Iyengar, Y. Dai, and M. Tomut, "A study of heavy ion beam induced damage in tungsten for high power target applications", in preparation.

[15] Luca Zanini, "The brightness per unit power of the ESS moderators at 570 MeV, 1.3 GeV and 2 GeV", Technical Report ESS-0090138, European Spallation Source ERIC, Jan. 2017